Theoretical Study of Aerosols Loading and Retention Over Bolgatanga, Ghana

Air, Soil and Water Research
Volume 10: 1–8

DOI: 10.1177/1178622117746995
SAGE

Emetere Moses E[1,2], Sanni SE[3] and Akinwumi SA[1]

[1]Department of Physics, Covenant University, Ota, Nigeria. [2]Mechanical Engineering Science, University of Johannesburg, Auckland Park, South Africa. [3]Department of Chemical Engineering, Covenant University, Ota, Nigeria.

ABSTRACT: The aerosols loading and retention over West Africa have grave effect on life-forms through the impact on health, farming, rainfall pattern, cloud formation, and regional climate. Bolgatanga can be found on the latitude and longitude of 10.78°N and 0.85°W, respectively. This research is focused on an investigative consideration of the negative effect of atmospheric aerosols over Bolgatanga in Ghana through a conceptual model using analytical and descriptive statistical methods with MATLAB curve-fitting tool. The model was verified using aerosol optical depth data set from satellite imagery—multi-angle imaging specto-reflectometer (MISR)—obtained over a period of 13 years. The highest percentage increase of aerosol retention was 64.27% over the research site. The model was used to estimate the atmospheric constants as 0.67, tuning constants as 0.24, and phase difference as $\pm\frac{\pi}{4}$. The physical interpretation of the results was analyzed systematically.

KEYWORDS: Aerosols retention, aerosols loading, climate, analytical technique, cloud formation

RECEIVED: April 2, 2016. **ACCEPTED:** November 15, 2017.

TYPE: Original Research

FUNDING: The author(s) received no financial support for the research, authorship, and/or publication of this article.

DECLARATION OF CONFLICTING INTERESTS: The author(s) declared no potential conflicts of interest with respect to the research, authorship, and/or publication of this article.

CORRESPONDING AUTHOR: Emetere Moses E, Department of Physics, Covenant University, Canaan land, P.M.B 1023, Ota 112211, Nigeria. Email: emetere@yahoo.com

Introduction

The impact of atmospheric aerosols in initializing climate change has been the focus of scientific discussion in recent times. Remote sensing technique is a very common method used by most scientists to gain insight into the larger view of the impact of atmospheric aerosols on climate change. Remote sensors basically read-off large volumes of spatial and temporal database of a given geographical region under study. For scientific applications, it is very important that the remotely sensed data sets are qualitative. For example, aerosols data set can be used to understand aerosol effects on atmospheric heat budget[1–4] and also for validating satellite measurements[5] and for model simulations.[6]

Aerosols comprise many components; however, dust particulate is a major component, and its dynamics in open space requires a systemic approach to model its dispersion, loading, precipitation, molecular interactions, and kinetics. In recent times, scientists have been able to show with proven degree of accuracy the properties of aerosols through dataset from Aerosol Robotic Network (AERONET), moderate resolution imaging spectroradiometer (MODIS), MISR, etc. For example, Dubovik et al[7] reported that through the information obtained from AERONET dataset, it was possible to retrieve aerosol size distribution, complex refractive index, and single-scattering albedo by inverting spectral optical depth together with sky radiances in the full solar almucantar. The information from other satellite stations, eg, MODIS and MISR has been proven to be very useful in atmospheric aerosol research. For example, Oluleye et al[8] showed that between 2005 and 2009, spatial, seasonal, and interannual variations of aerosol loading over some cities located in the Sahelian West Africa were detected by satellite (MODIS and Total Ozone Mapping Spectrometer [TOMS]) and ground-based AERONET Sunphotometer sensor. The daily, monthly, and annual aerosol optical properties of the MODIS were in good agreement with ground-based AERONET data.

Zhang et al[9] did the comparative review of algorithms used for air-quality models. The four areas that were considered include coagulation, condensational growth, nucleation, and gas particle mass transfer. The scientist observed that the condensational growth rate of particles was in the range of 0.001-10 μm. However, the review confirms the reliability of some models like CIT, GATOL, Models-3, SAQM-AERO, UAM-AERO, and UAM-AIM for handling coagulation and condensational growth of aerosol particulates. In the same vein, Anatoly et al[10] mathematically highlighted the removal of liquid aerosols from gases flowing through channels. This article showed that basic physical theorems were obeyed, eg, conservation of mass. Chan et al[11] presented an equilibrium kinetic model of secondary organic aerosols (SOA). They employed the model as a way of examining the effects of SOA formation in the gas phase oxidation of the products initially generated to more or less volatile species. The effect of pre-existing organic aerosol mass on SOA yield and its direct relevance to the translation of laboratory data for atmospheric applications were also examined. Four scenarios were considered in this kinetic study, and they include first-generation product with aerosol phase reacting, first-and-second-generation product with the unimolecular aerosol phase reacting with gas phase conversion to volatile second-generation product, first-and-second-generation semi-volatile product without the aerosol phase reacting, and volatile-first-generation product and semivolatile second-generation product. From the findings, it is evident that, while

different controlling/interacting mechanisms can lead to differing SOA growth behavior, it becomes generally impossible to deduce the actual mechanism for SOA formation with absolute dependence of the SOA growth data.

The article by Zuend et al[12] describes a liquid-liquid equilibrium and gas/particle partitioning model using the Aerosol Inorganic-Organic Mixtures. Functional groups Activity Coefficients (AIOMFAC) group-contribution model (Zuend et al, 2008)[13]. The model provides for the reliable computation of liquid-liquid coexistence (bimodal) curve, their corresponding tie-lines, the stability limit/meta-stability, and other thermodynamic properties of multicomponent systems. Thermodynamic evaluations of ternary and multicomponent alcohol/polyol-water-salt mixture properties suggest that liquid-liquid equilibrium is a prevalent feature of organic-inorganic aerosol systems. A multicomponent system was used to mimic the effects of relative humidity (RH) and the presence of liquid-liquid phase separation on the gas/particle partitioning. Based on their results, the model predictions revealed that liquid-liquid phase separation can lead to either an increase or decrease in total particulates of the entire mixture.

In recent times, the indiscriminate dispersion of atmospheric aerosols in cities located in West Africa has been proven via satellite imagery. In this article, further analysis on aerosols loading and retention was carried out over Bolgatanga to ascertain its level of pollution.

Theories: Statistical distribution

The SE of the mean was used (in this research) to estimate the population mean of aerosols for each month of the year. SE technique used for this research captures the standard deviation of the monthly means over one decade. The SE of the mean is expressed mathematically as

$$\mathrm{SE} = \frac{\sigma}{\sqrt{n}} \tag{1}$$

Here σ is the population standard deviation and n is the population size.

SE measures the uncertainty in aerosol optical depth (AOD) parameter and the deviations of the monthly mean from the average mean for the 13 years. Standard deviation (σ) measures the amount of visible dispersion from the monthly mean. Like the SE, a low-magnitude standard deviation signifies that the monthly mean is closer to the 13-year mean, which is also called the expected value. Also, a high magnitude standard deviation signifies how far the monthly mean is from the 13-year mean. Standard deviation is given as

$$\sigma = \sqrt{\frac{1}{N}\sum_{j=1}^{N}\left(y_i - \bar{y}\right)^2} \tag{2}$$

Here y_i in the context of our research is the monthly mean and $\bar{y}$ is the mean value of the 13-year mean. The concept of variance is intrinsically connected to the effects of the difference between the monthly mean and the 13-year mean on the AOD performance in Bolgatanga, Ghana. The coefficient of variation is the measure of a normalized dispersion of a probability distribution, ie, the 13 years mean for each parameter used. Coefficient of variation is referred to as relative standard deviation and expressed in percentage. Coefficient of variation is not used for measuring few meteorological parameters because of the inconsistency of its interval scale. Although the coefficient of variation is appropriate for the Kelvin scale and inappropriate for the Celsius scale because the Celsius scale is calibrated with an interval scale.[14] However, we adopted the coefficient of variation because the scale used has interval scale and appropriate for comparison between data sets of widely different yearly or monthly means. Coefficient of variation can be represented mathematically as

$$CV = \frac{\sigma}{\mu} \tag{3}$$

Here σ is the standard deviation and μ is the monthly mean. Skewness, also known as skew (X), is a measure of the asymmetry of the probability distribution of the monthly mean of aerosols about their 13-year mean. For a normal distribution, the skewness is equivalent to zero. The skewness value can be positive, negative, or undefined. When the skew is negative, it indicates that the mass of the distribution is concentrated on the right of the plotted graph, ie, left-skewed. When the skew is positive, the mass of the distribution is concentrated on the left of the plotted graph, ie, right-skewed. The skew of a distribution can be written mathematically as

$$X = \frac{\left(\mu - \upsilon\right)}{E\left(\left|X - \upsilon\right|\right)} \tag{4}$$

Here υ is the median and E is the expectation error.

Kurtosis (β) is any measure of the flattening or "peakedness" of the probability distribution of the monthly mean for each month of the year. Like skewness, kurtosis is a descriptor of the shape of a probability distribution which can be interpreted as $\beta > 3$ (leptokurtic distribution—high probability for extreme values), $\beta < 3$ (platykurtic distribution—probability for extreme values is less than for a normal distribution), and $\beta = 3$ (mesokurtic distribution—normal distribution). Kurtosis mathematically written as

$$\beta = \frac{\mu^4}{\sigma^4} \tag{5}$$

All parameters retain their usual meanings. The simulation was carried out using analytical tool.

Validation of data source

Bolgatanga is the fourth most populous city in northern Ghana, and it is located on longitude 0.85°W and latitude 10.78°N in

Figure 1. Map of Bolgatanga and the Sahara influence.

the Sahelian geographic region south of the Sahara (Figure 1); hence, we expect a high impact of the northeast winds along with the Sahara dust. It is also under the influence of the local steppe climate. Its metropolitan area is about 499 km^2. Bolgatanga has average temperature and precipitation of 26.1°C and 752 mm, respectively. The distance of Bolgatanga is about 2826 km. In the past, no aerosols ground observation was available; hence, the satellite observation was adopted. Fourteen years satellite observation was obtained from the MISR. The MISR operates at various directions, ie, nine different angles (70.5°, 60°, 45.6°, 26.1°, 0°, 26.1°, 45.6°, 60°, and 20.5°) and gathers data in four different spectral bands (blue, green, red, and near-infrared) of the solar spectrum. The blue band is at wavelength 443 nm, the green band is at wavelength 555 nm, the red band wavelength is 670 nm, and the infrared band is at wavelength 865 nm. MISR acquires images at two different levels of spatial resolution, ie, local and global modes. It gathers data at the local mode at 275 m pixel size and 1.1 km at the global mode. Typically, the blue band is to analyze coastal and aerosol studies. The green band is for bathymetric mapping examination and to estimate peak vegetation. The red band analyzes the variable vegetation slopes, and the infrared band analyzes the biomass content and shorelines.

Methodology

The raw MISR dataset was processed using Excel. The mean for each month was calculated all through each year. The accuracy of the data by applying the aerosol dispersion model that was propounded by Emetere et al[15] was verified. An extension of the dispersion model used is given as

$$\psi(\lambda) = a_1^2 \cos\left(\frac{n_1 \pi \tau(\lambda)}{2} + \alpha\right)\cos\left(\frac{n_1 \pi \tau(\lambda)}{2} + \beta\right) + \ldots\ldots a_n^2 \cos\left(\frac{n_n \pi \tau(\lambda)}{2} + \alpha\right)\cos\left(\frac{n_n \pi \tau(\lambda)}{2} + \beta\right) \quad (6)$$

Here α and β are the phase differences, τ is the AOD, ψ is the concentration of contaminant, λ is the wavelength, and a and n are atmospheric and tuning constants, respectively.

The percentage of retention can be determined from the coefficient of variance for each year. This was done by considering the previous and current years which are denoted as G_P and G_r, respectively. Hence, the aerosols retention between 2 years is propounded as

$$A = \left|\frac{G_r - G_P}{G_r}\right|^2 \times 100\% \quad (7)$$

The aerosols retention can be calculated from Tables 2 and 3 to obtain Tables 4 and 5. Any statistical tool could be used to obtain the atmospheric aerosols retention.

Results and Discussion

The Bolgatanga monthly AOD trend agreed perfectly with the proposed model (Figures 2 to 4). More importantly is that it showed the mathematical distribution patterns. For example, AOD pattern over Bolgatanga is a gamma distribution with the maximum in March. This further affirms that the type of aerosols in the area are majorly dust particulates (Figure 4). It is easy to explain this via the influence of the northeast wind. Accuweather (2015) showed that Bolgatanga has a more stable weather compared to other parts of the country. Hence, it will be easier to calculate its AOD retrieval over a given period of time.

From the monthly AOD distribution in Figure 2, the AOD for the year 2000 dropped from January to March. It rose to a peak in April and dropped in the month of May and was fairly constant through June after which it rose to a peak in July and dropped in August. A slight increase can be observed from August through to October. In the year 2001, the AOD rose from 0.44 in January to 1.5 in March. It dropped through April to 0.42 in May. It was 0.7 in June and dropped to 0.62 in July. A further drop in AOD was recorded for the month of August after which a rise and fall in AOD was experienced for the remaining months all through to December. In 2002, the AOD dropped from 1 to 0.48 in January and February, respectively. It peaked at 1.2 in the month of March and dropped through April to 0.5 in May and remained fairly constant through May to June and dropped to 0.3 in August. It rose through August and September to a peak of 0.7 in October and dropped subsequently through November to 0.3 in December. In the year 2003, the AOD rose from 0.42 in January to 0.6 in February. It was 1.0 in March and dropped through April to 0.5 in May. The AOD for June was 0.8 after which it dropped to 0.3 in July. There was a slight increase in the AOD from 0.4 in August to 0.5 in September with subsequent rise and fall in AOD through October down to December. In 2004, the AOD was 0.58 in January. It rose through February bending through a maximum in March at 0.98 and dropped slightly to 0.9 in April. A significant drop in AOD is seen in the month of May with AOD value of 0.5. It remained constant at 0.5 through June and dropped to 0.4 in July. The AOD rose through August to 0.5, dropped to 0.4 in September with continuous increase in the AOD down to December. For the year 2005, the AOD was 0.6 in January and 1.8 in February. It was 0.82 in March and 1.1 in April. It then dropped through May to 0.6 in June and was quite low in through July to September and October

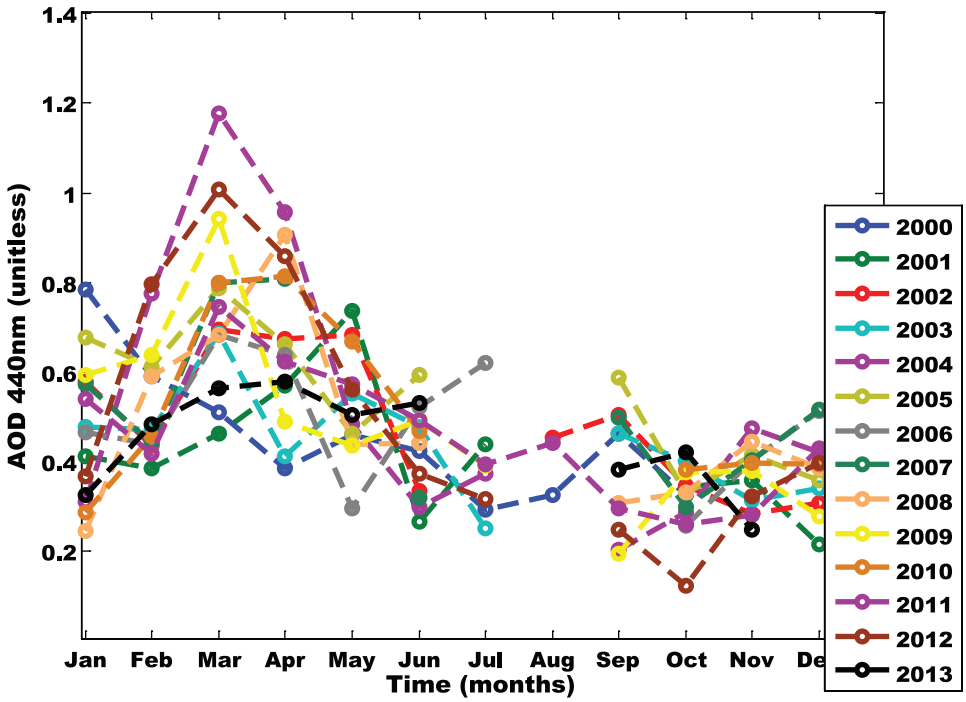

Figure 2. AOD pattern for Bolgatanga (2000-2013).

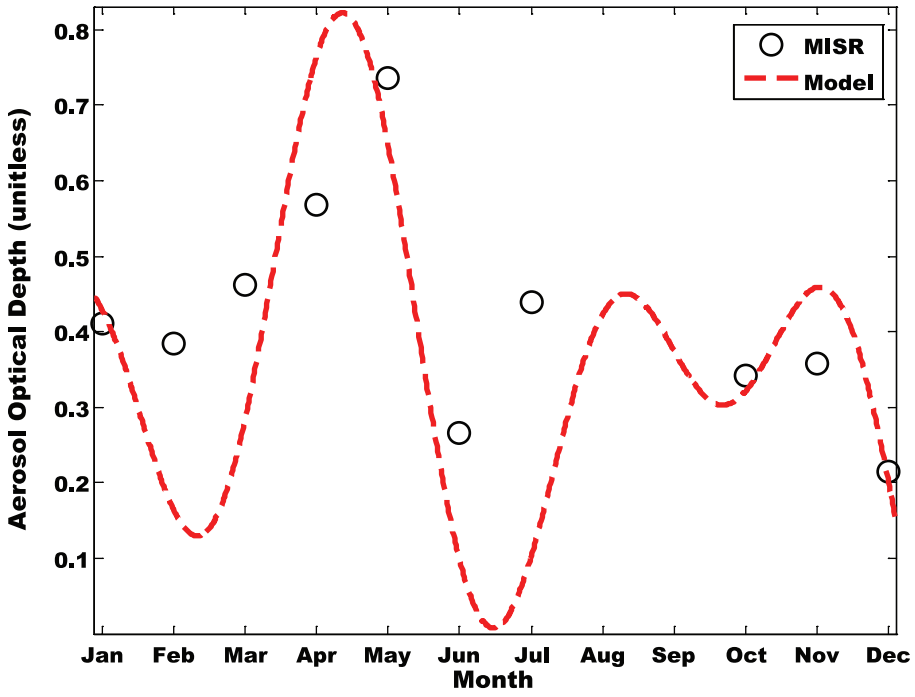

Figure 3. AOD for new model and MISR for the year 2000.

where the AOD was 0.4 with an increase of 10% in November. In 2006, the values of the AODs are 0.44, 0.5, and 1.15 for the months of January, February, and March, respectively. It was 0.62 and 0.42 in April and May, respectively, while it continued to rise and drop all through June to December with an AOD of 0.5. In 2007, the AOD was 0.72 in January. It dropped to 0.62 in February and rose to 1 in March. It dropped to 0.8 and 0.6 in April and May, respectively, and remained lower than 0.6 for the remaining months through to December. In 2008, the highest AOD was recorded in the month of February as 0.9 which is 10% higher than the AOD recorded in January. It was 0.66 in March and remained fairly constant through April after which it continued to drop until August. The AOD for September through to December were 0.6, 0.26, 0.6, and 0.4, respectively. In 2009, the highest AOD (0.8) was recorded in the month of July and it continued to fall and rise subsequently through to the December. The year 2010 shows a rise in the AOD from January to March where the highest AOD of 1.3

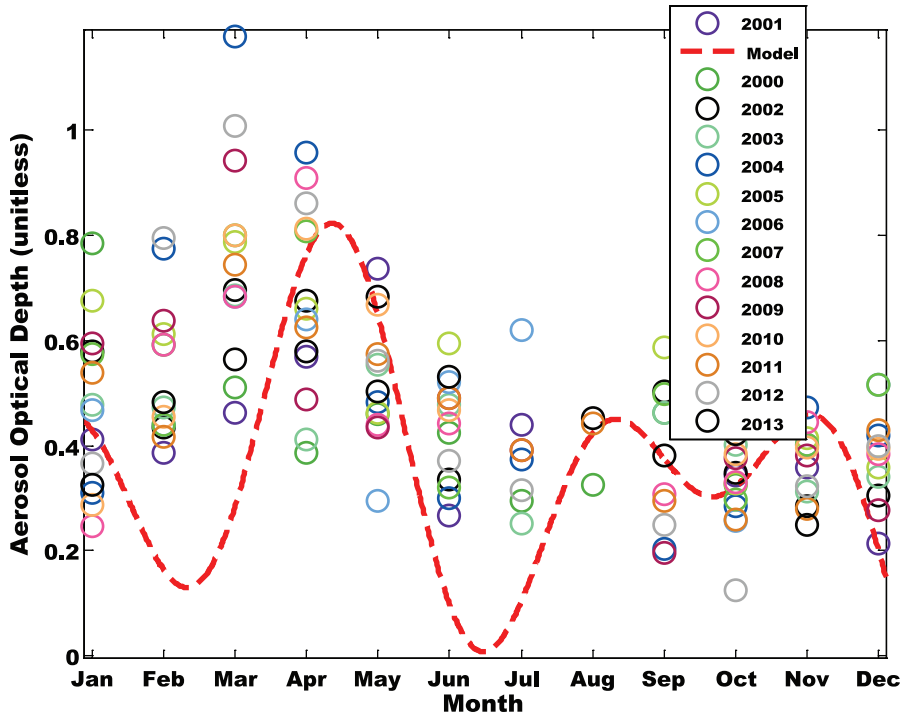

Figure 4. Analysis of the model to capture the AOD trends.

was obtained. It was 0.5 in May and rose to 0.6 in June. It was lower than 0.6 for other months down to November where the AOD was 0.32 and rose slightly to 0.4 in December.

For AOD records in 2011, a rise in AOD can be seen in Figure 2 where it rose from 0.42 in January through February and March to April. It was 0.6 in June and July and was lower for other months, except in December where it was the same value as recorded in the months of June and July. In 2012, the AOD was 0.4 and rose through February to 1.0 in March after which it continued to drop down to July where it was 0.5. It rose to 0.6 in August and was 0.3 in September after which it was fairly constant at 0.5 from October through November to December. The highest AOD recorded in the year 2013 was 0.78, and this was for the month of April. It dropped from 0.7 in January through to March where it was 0.5. It dropped in May to 0.56 and rose slightly to 0.6 in June. It dropped through July to 0.3 in August. It was 0.66 in September and remained fairly constant at 0.4 between October and November. The month of December seemed to be free of aerosols for that year. The data generated could be described as one exhibiting a wave-form.

Figures 3 and 4 give the model predictions and the data generated from satellite. In Figure 3, the aerosol optical depths as obtained from the satellite (MISR) images agree with the AOD predictions of the model for the year 2000 for all other months except that slight deviations can be seen in the months of July, August, October, and November. In Figure 4, the AOD estimated for the year 2002 by the model seems to agree with those of the MISR for all other 8 months. There is a clear deviation in March and slight deviations in the months of May, June, October, November, and December. Figure 4 shows the AOD estimates in the year 2007 for the model against data generated by satellite imaging. The model estimates agree with the satellite images for other months except for the deviations seen in the months of January, March, May, July, August, September, and November. In Figure 4, for the year 2011, there are deviations of the estimated AODs for the months of January, March, May, June, August, and November with only a few points in agreement, ie, those of February, April, May, July, September, and December.

Table 1. Atmospheric constants over Bolgatanga.

LOCATION	a_1	a_2	n_1	n_2	α	β
Bolgatanga	0.667	0.6403	0.242	0.1515	$\pm\frac{\pi}{4}$	$\pm\frac{\pi}{4}$

From Figures 2 to 4, the atmospheric constants, phase differences, and tuning constants can be obtained from the MATLAB curve fit tool and equation (6) as shown in Table 1 below. The methods of obtaining constants from MATLAB fitting is explained in Danilo.[16]

It is important to note that this article focuses on the reliability of the International Telecommunication Union Recommendation (ITU-R) model because it suggests an alteration in its known[17] model shown in equation (8):

$$N = \frac{77.6P}{T} + 3.73\times10^{5}\frac{e}{T^2} = N_{dry} + N_{wet}\left(N - units\right) \quad (8)$$

Where N is the refractivity, e is the water vapor pressure, P is the atmospheric pressure (hPa), and T is the absolute

Table 2. Statistical AOD analysis 2000-2006.

STATISTICAL TOOL	2000	2001	2002	2003	2004	2005	2006
SE	0.047	0.047	0.047	0.036	0.094	0.048	0.045
95% confidence interval	0.105	0.107	0.105	0.08	0.209	0.108	0.101
99% confidence interval	0.151	0.154	0.15	0.114	0.298	0.155	0.146
Variance	0.022	0.022	0.025	0.014	0.097	0.023	0.02
Standard deviation	0.147	0.149	0.157	0.119	0.312	0.15	0.142
Coefficient of variation	0.323	0.357	0.326	0.271	0.595	0.275	0.293
Skew	1.258	0.945	0.236	0.468	1.234	−0.12	−0.231
Kurtosis	1.799	1.326	−1.588	0.818	0.526	−1.05	−0.845
Kolmogorov-Smirnov stat	0.185	0.184	0.168	0.196	0.279	0.203	0.132

AOD: aerosol optical depth.

Table 3. Statistical AOD analysis 2007-2013.

STATISTICAL TOOL	2007	2008	2009	2010	2011	2012	2013
SE	0.062	0.063	0.061	0.064	0.042	0.085	0.038
95% confidence interval	0.142	0.142	0.135	0.148	0.093	0.189	0.087
99% confidence interval	0.207	0.205	0.192	0.216	0.131	0.269	0.126
Variance	0.034	0.04	0.04	0.037	0.021	0.079	0.013
Standard deviation	0.185	0.199	0.201	0.193	0.146	0.281	0.113
Coefficient of variation	0.358	0.417	0.424	0.372	0.319	0.576	0.251
Skew	0.689	1.204	1.164	0.723	0.437	0.794	−0.646
Kurtosis	−0.56	1.282	2.211	−1.08	−0.23	−0.54	−0.624
Kolmogorov-Smirnov stat	0.172	0.266	0.193	0.271	0.125	0.262	0.176

AOD: aerosol optical depth.

temperature (K). The mathematical relationship between RH and water vapor pressure is expressed in the following equation:

$$e = \frac{RH}{100} a \, exp\left[\frac{bT}{T+c}\right] \quad (9)$$

Here, the temperature T in the above equation is given in °C and the coefficients a, b, and c are given as follows: a = 6.1121, b = 17.502, and c = 240.97. The implication of this research on the understanding of the results from Leck and Svensson[18] is that the determination of coefficients a, b, and c is influenced by the optical state over a geographical location. This study proposes an inclusion of the attenuation due to moving aerosols layer into the ITU model which is significant via the atmospheric constants over Bolgatanga. By this concept, we statistically examined the AOD distribution over Bolgatanga as shown in Tables 2 and 3.

The highest AOD mean, 95% confidence interval, 99% confidence interval, variance, standard deviation, and coefficient of variation were obtained in 2005. The highest skew and kurtosis can be sited in year 2010. The highest Kolmogorov-Smirnov stat can be found in 2004. The results show that the lower atmosphere of Bolgatanga may not be as dynamic as those of cities in southern Nigeria.[19] Hence, we examined the atmospheric aerosol retention shown in Table 4.

Considering the data in Table 2, the estimated variances show that the highest deviation of the estimated monthly means from the 13-year mean was obtained for the year 2005 which reveals that it is farthest from the 13-year mean with that of 2001 showing the least deviation. From the estimated standard deviations, it is clear that the amount/degree of aerosol dispersion of the monthly means from the 13-year mean is lowest for the year 2001 with the highest seen in the year 2005; those of other years lie between these values. The coefficient of variation or the degree of

Table 4. Atmospheric aerosols retention over Bolgatanga 2001-2006.

	2001	2002	2003	2004	2005	2006	
Aerosol deposition	1.13	0.76	2.89	29.72	29.02	0.44	
Aerosol deposition	2007	2008	2009	2010	2011	2012	2013
	4.89	2.75	0.03	1.51	2.01	64.27	31.73

normalized dispersion of aerosols is highest in the year 2005 with a value of 0.46 with an average population of aerosols of 0.63 having confidence of 20% and 28% within the 95% and 99% confidence intervals. For the calculated skews, it could be seen that the measure of asymmetry of the probability distribution of the monthly means of the aerosols about the 13-year mean shows that the aerosol distribution has all the aerosol mass concentrated on or distributed to the left side of the plots for all the years; it is highest for the years 2000 and 2006 but lowest for the year 2001. Based on the calculated kurtosis for all the years, it can be deduced that the probability distribution of aerosols for all the years is platykurtic in shape because the estimated values are all less than 3. Also, because the probability of the extreme values, ie, 0.75 for the year 2000 and 2.46 for the year 2006, it then implies that the estimated probabilities of the extreme values are less than that of a normal distribution. Furthermore, from the estimated values, it could be seen that the highest peaks and degree of flattening were obtained in the year 2006 while the least was that of 2001.

Similarly, a look at the data in Table 3 shows that the highest deviation or variance (0.08) of the estimated monthly means from the 13-year mean was obtained for the year 2010, which reveals that it is farthest from the 13-year mean while those of 2011 and 2012 show the least deviation (0.03 each). From the estimated standard deviations, it is clear that the amount/degree of aerosol dispersion of the monthly means from the 13-year mean is lowest (0.17 each) for the years 2011 and 2013 with the highest dispersion (0.28) seen in the year 2010; those of other years lie between these values. The coefficient of variation or the degree of normalized dispersion of aerosols is highest for the year 2010 with a value of 0.49 with an average population of aerosols of 0.57 having confidence of 19% and 26% within the 95% and 99% confidence intervals, respectively. For the calculated skews, it could be seen that the measure of asymmetry of the probability distribution of the monthly means of the aerosols about the 13-year mean shows that the aerosol distribution has all the aerosol mass concentrated on or distributed to the left side of the plots for all the years except for that of year 2009 which is concentrated to the left; it is highest (1.93) for the year 2010 but lowest for the year 2009 with a value of −0.2. Based on the calculated kurtosis for all the years, it can be deduced that the probability distribution of aerosols for all other years except 2010 is platykurtic in shape. For 2010, it is a leptokurtic distribution because the estimated kurtosis value is 4.38, which is greater than 3. Also, because the kurtosis of the extreme values, ie, −1.6 for the year 2009 and 4.38 for the year 2010, it then implies that the estimated probabilities of the extreme values are less than that of a normal distribution for other years but highly distributed in the year 2010. Furthermore, from the estimated values, it could be seen that the highest peakedness and degree of flattening were obtained in the year 2010 while the least was that of 2009.

Considering Tables 4, the years of highest values of atmospheric aerosols retention were found to be 2012 and 2013. This shows that the skew and kurtosis are good indicators of atmospheric aerosols retention. More so, the trend of the aerosol retention shown in Table 4 is an evidence of indiscriminate anthropogenic pollution in its atmosphere. For example, the retention in 2004 and 2005 was high compared with the results between 2001 and 2011. The significance of the atmospheric aerosols retention in a geographical region has great influence on aviation schedules,[20] human health,[21] measuring instruments, energy budget, and meteorology.[22] Hence, the trends of the aerosol retention over Bolgatanga is of immense interest to environmental authorities within the region.

Conclusion

The new model has shown accuracy to describe the physical properties of aerosols—in relation to the dispersion type. Its validation with satellite dataset shows that it is reliable based on the statistical outcomes. The limitation of the study was highlighted for its further improvement. The platykurtic and leptokurtic aerosol distributions in Bolgatanga show that it is becoming more difficult to access the volume of air pollution released into the atmosphere. Hence, this study strengthens the World Health Organization (WHO) red alert on some cities in Africa. The maximum aerosol retention was 64.27%. Its atmospheric constants, tunning constants, and the phase difference over Bolgatanga was found to be 0.67, 0.24, and $\pm\frac{\pi}{4}$, respectively. Further research on the predictive nature of the model is recommended for similar climate system.

Acknowledgements

The authors acknowledge the partial sponsorship of Covenant University. The authors appreciate the contribution of NASA for the satellite data set used in this research.

Author Contribution

EME designed and wrote the framework. SSE contributed to the write-up and ASA edited the manuscript.

REFERENCES

1. Aoki K, Fujiyoshi Y. Sky radiomter measurements of aerosol optical properties over Sapporo, Japan. *J Meteorol Soc Jpn*. 2003;81:493–513.
2. Kim DH, Sohn BJ, Nakajima T, Takamura T. Aerosol radiative forcing over East Asia determined from ground-based solar radiation measurements. *J Geophys Res*. 2005;110:D10S22. doi:10.1029/2004JD004678.
3. Uchiyama A, Yamazaki A, Togawa H, Asano J. Characteristics of aeolian dust observed by sky-radiometer in the Intensive Observation Period 1 (IOP1). *J Meteorol Soc Jpn*. 2005;83:291–305.
4. Takamura T, Sugimoto N, Shimizu A, et al. Aerosol radiative characteristics at Gosan, Korea, during the atmospheric brown cloud East Asian regional experiment 2005. *J Geophys Res*. 2008;112:D22S36. doi:10.1029/2007JD008506.
5. Higurashi A, Nakajima T, Holben BN, Smirnov A, Frouin R, Chatenet B. A study of global aerosol optical climatology with two channel AVHRR remote sensing. *J Climate*. 2000;13:2011–2027.
6. Takemura T, Okamoto H, Maruyama Y, Numaguti A, Higurashi A, Nakajima T. Global three-dimensional simulation of aerosol optical thickness distribution of various origins. *J Geophys Res*. 2000;105:853–873.
7. Dubovik O, Smirnov A, Holben BN, et al. Accuracy assessments of aerosol optical properties retrieved from Aerosol Robotic Network (AERONET) Sun and sky radiance measurements. *Geophys Res*. 2000;105:9791–9806.
8. Oluleye A, Ogunjobi KO, Benard A, Ajayi V, Akinsanola AA. Multiyear analysis of ground-based sunphotometer (AERONET) aerosol optical properties and its comparison with satellite observations over West Africa. *Global J Human Soc Sci Geo Environ Geosci*. 2012;12:1–29.
9. Zhang Y, Seigneur C, Seinfeld JH, Jaconson MZ, Binkowski FS. Simulation of aerosol dynamics: a comparative review of algorithms used in air quality models. *Aerosol Sci Tech*. 1999;31:487–514.
10. Laptev AG, Basharov MM, Farakhov TM, Iskhakov AR. Calculating efficiency of separation of aerosol particles from gases in packed apparatuses. *Adv Chem Eng Sci*. 2014;2014:143–148.
11. Chan AWH, Kroll JH, Ng NL, Seinfeld JH. Kinetic modeling of secondary organic aerosol formation: effects of particle- and gas-phase reactions of semi-volatile products. *Atmos Chem Phys*. 2007;7:4135–4137.
12. Zuend A, Marcolli C, Peter T, Seinfeld JH. Computation of liquid-liquid equilibria and phase stabilities: implications for RH-dependent gas/particle partitioning of organic-inorganic aerosols. *Atmos Chem Phys*. 2010;10:7795–7820.
13. Zuend A, Marcolli C, Luo B P, and Peter, T. A thermodynamic model of mixed organic-inorganic aerosols to predict activity coefficients. *Atmos Chem. Phys*. 2008;8:4559–4593.
14. Geddes SM. Measurement of temperature. *Adv Phys*. 1981:2–10 (London, England: Palgrave Macmillan). https://doi.org/10.1007/978-1-349-04806-9_1
15. Emetere ME, Akinyemi ML, Akinojo O. Parametric retrieval model for estimating aerosol size distribution via the AERONET, LAGOS station. *Environ Pollut*, 2015;207:381–390.
16. Danilo S. Solving equations and curve fitting—MIT OpenCourseWare. https://webcache.googleusercontent.com/search?q=cache:h6rwMKoyYpkJ:https://ocw.mit.edu/courses/electrical-engineering-and-computer-science/6-094-introduction-to-matlab-january-iap-2010/lecture-notes/MIT6_094IAP10_lec03.pdf+&cd=1&hl=en&ct=clnk&gl=za&client=firefox-b-ab
17. ITU-R. *The Radio Refractive index: its Formula and Refractivity Data*. Geneva, Switzerland: ITU-R; 2015.
18. Leck C, Svensson E. Importance of aerosol composition and mixing state for cloud droplet activation over the Arctic pack ice in summer. *Atmos Chem Phys*. 2015;15:2545–2568.
19. Emetere ME, Akinyemi ML, Akin-Ojo O. Aerosol optical depth trends over different regions of Nigeria: thirteen years analysis. *Mod Appl Sci*. 2015;9: 267–279.
20. Gettelman A, Chen C. The climate impact of aviation aerosols. *Geophys Res Lett*. 2013;40:2785–2789.
21. Wyzga RE, Folinsbee LJ. Health effects of acid aerosols. *Water Air Soil Pollut*, 1995;85:177–188.
22. Emetere ME, Akinyemi ML. Modeling of generic air pollution dispersion analysis from cement factory. *Analele Univ din Oradea–Seria Geo*. 2013;1:181–189.